

DISKS CONTROLLING CHAOS IN A 3D DYNAMICAL MODEL FOR ELLIPTICAL GALAXIES

Euaggelos E. Zotos

*Department of Physics, Section of Astrophysics, Astronomy and Mechanics,
Aristotle University of Thessaloniki, 541 24, Thessaloniki, Greece;
evzotos@astro.auth.gr*

Received: 2011 February 13; revised: March 23; accepted: March 31

Abstract. A 3D dynamical model with a quasi-homogeneous core and a disk component is used for the chaos control in the central parts of elliptical galaxy. Numerical experiments in the 2D system show a very complicated phase plane with a large chaotic sea, considerable sticky layers and a large number of islands, produced by secondary resonances. When the mass of the disk increases, the chaotic regions decrease gradually, and, finally, a new phase plane with only regular orbits appears. This evolution indicates that disks in elliptical galaxies can act as the chaos controllers. Starting from the results obtained in the 2D system, we locate the regions in the phase space of the 3D system, producing regular and chaotic orbits. For this we introduce and use a new dynamical parameter, the $S(w)$ spectrum, which proves to be useful as a fast indicator and allows us to distinguish the regular motion from chaos in the 3D potentials. Other methods for detecting chaos are also discussed.

Key words: galaxies: kinematics and dynamics – galaxies: elliptical

1. INTRODUCTION

Today it is believed, that dwarf elliptical galaxies seem to prefer the densest regions of the Universe and are found abundantly in galaxy clusters and groups (see Bingelli et al. 1987; Ferguson & Sandage 1989; Conselice et al. 2001). This circumstance most likely has important consequences for their evolution. Moore et al. (1998) have shown how late-type disk galaxies, that orbit in a cluster, can lose angular momentum by interactions with massive galaxies and, to a lesser degree, by tidal forces induced by the cluster potential. N -body simulations performed by Mayer et al. (2001) show that small disk galaxies, that are close companions to a massive galaxy, will be affected likewise. A small disk galaxy is destabilized and develops a bar that gradually slows down, by dynamical friction, transporting angular momentum to the halo and to stars at larger radii. Since the latter are being stripped, angular momentum is lost. Gas is funneled in towards the center by torques exerted by the bar, where it is converted into stars, thus forming a nucleus. The small companion is heated by the subsequent buckling of the bar (see Merrifield & Kuijken 1999 and references therein) and by bending modes of the disk, and is transformed from a rotationally-flattened object into an anisotropic, slowly rotating spheroidal galaxy. The effect on a dwarf galaxy depends on its

orbit through the cluster around the massive companion. For instance, retrograde interactions have a much less damaging effect than prograde ones and may even preserve some of the initial disk structure. Thus, these simulations allow for the existence of fast-rotating dwarfs and for elliptical galaxies that still contain a stellar disk.

During the last decade, dwarf elliptical galaxies, such as IC 3328, IC 0783, IC 3349, NGC 4431 and IC 3468, with spiral and barred structure have been discovered in the Virgo cluster (see Jerjen et al. 2000; De Rijcke et al. 2001; Barazza et al. 2002; Simien & Prugniel 2002). Furthermore, Ryden et al. (1999) also report dwarf ellipticals with disk-like isophotes in the Virgo cluster, while De Rijcke et al. (2003) give photometric evidence for the presence of stellar disks in two Fornax dwarf galaxies FCC 204 and FCC 288. Moreover, there are indications of the presence of disks in the giant elliptical galaxies NGC 83 and NGC 2320 (see Young 2002, 2005). The semi-analytic simulations of Khochfar & Burkert (2005) suggest that a few tens of percent of all disk elliptical galaxies, could have grown their stellar disks out of cold gas accreted from the intergalactic medium. A better understanding of the molecular gas in early-type galaxies could provide concrete evidence either for or against this disk scenario.

Taking this into account, we considered interesting to construct a 3D dynamical model to study properties of the motion in an elliptical galaxy with a disk. In order to describe the motion in the region near the center of such a system, we use the potential

$$V(x, y, z) = \frac{\omega^2}{2} [(x^2 + by^2 + cz^2) - \epsilon x (y^2 + z^2)] - \frac{M_d}{\sqrt{x^2 + y^2 + (\alpha + \sqrt{h^2 + z^2})^2}}. \quad (1)$$

Potential (1) consists of two parts. The first term stands for the quasi-homogeneous core of the galaxy, the second term describes the disk (see Miyamoto & Nagai 1975). The harmonic term of the potential is valid only within certain distances from the center of the galaxy. In our case, integration of orbits was done up to distances $R = \sqrt{x^2 + y^2 + z^2} \leq 1$, hinting that up to these distances from the galactic center, the harmonic term of Eq. (1) is valid. We must point out, that the perturbation term ($-\epsilon x (y^2 + z^2)$) of the harmonic potential is an odd function with respect to x . We use this kind of perturbation term due to the fact that it has a finite energy of escape. Moreover, the first term of potential (1) is a deformed galactic model, which is approximately axisymmetric near the core but is deformed in its outer parts. A two-dimensional potential with this kind of perturbation was used by Contopoulos et al. (1987) in order to study large-scale stochasticity in a Hamiltonian system of two degrees of freedom, which may represent the inner parts of a deformed galactic model. In the present paper, the first term of potential (1), is the expansion of the potential used by Contopoulos et al. (1987) in a Hamiltonian system of three degrees of freedom. Similar potentials have been used in several papers, in order to study axisymmetric galactic models (see Contopoulos & Polymilis 1993; Siopis et al. 1995).

In Eq. (1), b , c and ϵ are parameters, M_d is the mass, a and h are the scale length and the scale height of the disk, while ω is used for the consistency of the galactic units. We use a system of galactic units, where the unit of mass is $2.325 \times 10^7 M_\odot$, the unit of length is 1 kpc and the unit of time is 0.997748×10^8 yr. The velocity unit is 10 km/s, while G is equal to unity. In the above units we

use the values: $\omega = 10 \text{ km s}^{-1} \text{ kpc}^{-1}$, $b = 1.1$, $c = 1.5$, $\epsilon = 1.08$, $\alpha = 3$, $h = 0.125$, while M_d is treated as a parameter.

The aim of this research is to investigate the role, played by the disk, on the regular or chaotic nature of orbits. Our investigation will be focused in the following: (i) we will try to connect the extent of the chaotic regions with the mass of the disk; (ii) we will look for sticky regions and secondary resonances introduced by the presence of the disk, and (iii) we will seek if there exist only one unified chaotic region, or different chaotic components. For this purpose, we shall use, apart of the classical methods, such as the Poincaré phase plane and the Lyapunov Characteristic Exponents (LCEs) (Lichtenberg & Lieberman 1992), some modern methods such as the $S(c)$ spectrum (Caranicolas & Papadopoulos 2007; Caranicolas & Zotos 2010), the $P(f)$ indicator (Karanis & Vozikis 2008) and a new dynamical parameter, the $S(w)$ spectrum.

The results are based on the numerical integration of the equations of motion

$$\begin{aligned}\ddot{x} &= -\frac{\partial V(x, y, z)}{\partial x}, \\ \ddot{y} &= -\frac{\partial V(x, y, z)}{\partial y}, \\ \ddot{z} &= -\frac{\partial V(x, y, z)}{\partial z}.\end{aligned}\quad (2)$$

The Hamiltonian to the potential (2) reads

$$H = \frac{1}{2} (p_x^2 + p_y^2 + p_z^2) + V(x, y, z) = E, \quad (3)$$

where p_x, p_y, p_z are the momenta per unit mass conjugate to x, y and z , while E is the numerical value of the Hamiltonian.

The orbit calculations are based on the numerical integration of the equation of motion (2), which was made using a Bulirsh-Stöer routine in Fortran 95, with double precision in all subroutines. The accuracy of the calculations was checked by the consistency of the energy integral (3), which was conserved up to the twelfth significant figure.

The present paper is organized as follows: in Section 2 we present an analysis of the structure of the $x - p_x, y = 0, p_y > 0$ Poincaré phase plane of the 2D system and the different families of orbits. In the same section a study of the evolution of the sticky regions is presented. Moreover, we investigate the evolution of different chaotic components of the system. In Section 3 we study the character of orbits in the 3D system, using a new dynamical indicator, the $S(w)$ spectrum. Special interest is given to the evolution of the sticky regions and the chaotic components. In Section 4, a discussion and the conclusions of this research are presented.

2. THE STRUCTURE OF THE $x - p_x$ PHASE PLANE: CHAOTIC COMPONENTS AND STICKY REGIONS

In this section we will analyze the structure of the $x - p_x, y = 0, p_y > 0$ Poincaré phase plane of the corresponding 2D potential, i.e., we will consider orbits on the galactic plane ($z = 0$). The corresponding Hamiltonian is

$$H_2 = \frac{1}{2} (p_x^2 + p_y^2) + V(x, y) = E_2, \quad (4)$$

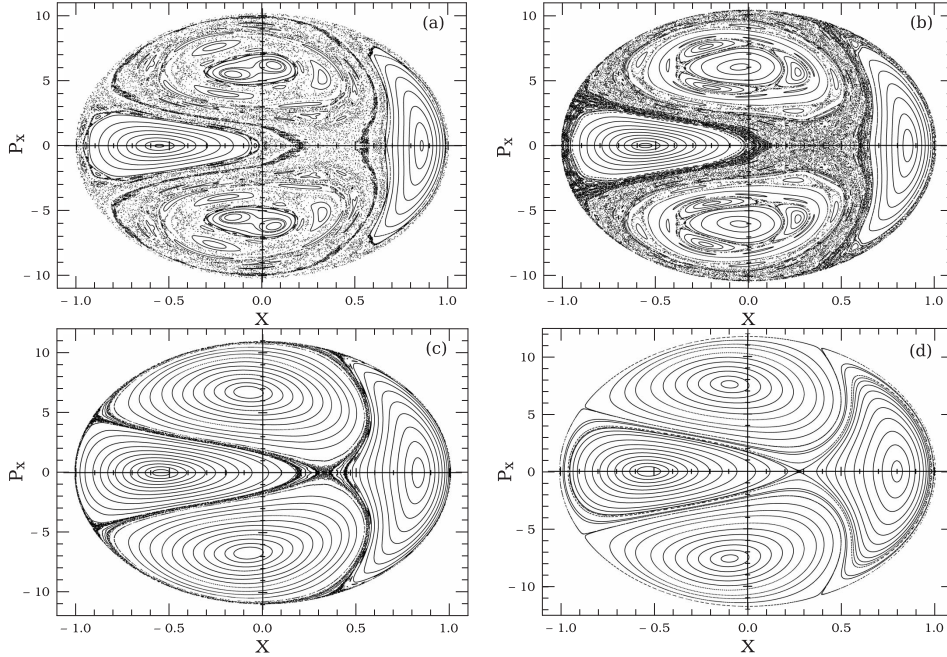


Fig. 1. The $x - p_x$ phase plane. Panel (a): $M_d = 100$, $E_2 = 20$; panel (b): $M_d = 200$, $E_2 = -10$; panel (c): $M_d = 600$, $E_2 = -132$; panel (d): $M_d = 1200$, $E_2 = -315$.

where E_2 is the numerical value of the Hamiltonian.

Figures 1 (a-d) show the $x - p_x$ phase plane of the 2D system. Let us start from Figure 1a, where $M_d = 100$, $E_2 = 20$. One observes a phase plane with a complicated structure. Several chaotic components seem to exist. There are also two main regions of regular motion. The first regular region, forms invariant curves around the two invariant points on the x -axis, while the second region is composed of two sets of islands intersecting the p_x -axis. Both the above islands are produced by quasi-periodic orbits characteristic of the 1:1 resonance. A considerable regular region is occupied by two additional sets of three islands symmetrical with respect to the x -axis. Furthermore, there are sets of smaller islands embedded in the chaotic sea and produced by secondary resonances. Several sticky regions seem to be present, but we shall come to this interesting point later in this Section. Figure 1b shows the phase plane when $M_d = 200$, $E_2 = -10$. At a first glance, we see that the regular region has increased, while the chaotic regions have decreased. Note that the two invariant points near the p_x -axis are now stable. The chaotic components are present in this case too. The different chaotic components will be studied later in this Section. We must also point out, that in this case we can see one main sticky region and some smaller secondary sticky regions as well. Figure 1c shows the $x - p_x$ phase plane in the case when $M_d = 600$, $E_2 = -132$. Here things are different. Almost the entire phase plane is regular, while only a small chaotic layer with some tiny sticky regions is observed. On the other hand, all periodic points are now stable, and no secondary resonances are observed. Figure 1d is similar to Figure 1c, but for $M_d = 1200$, $E_2 = -315$. In this case, the entire phase plane is covered by regular orbits, while the percentage of chaotic orbits, if

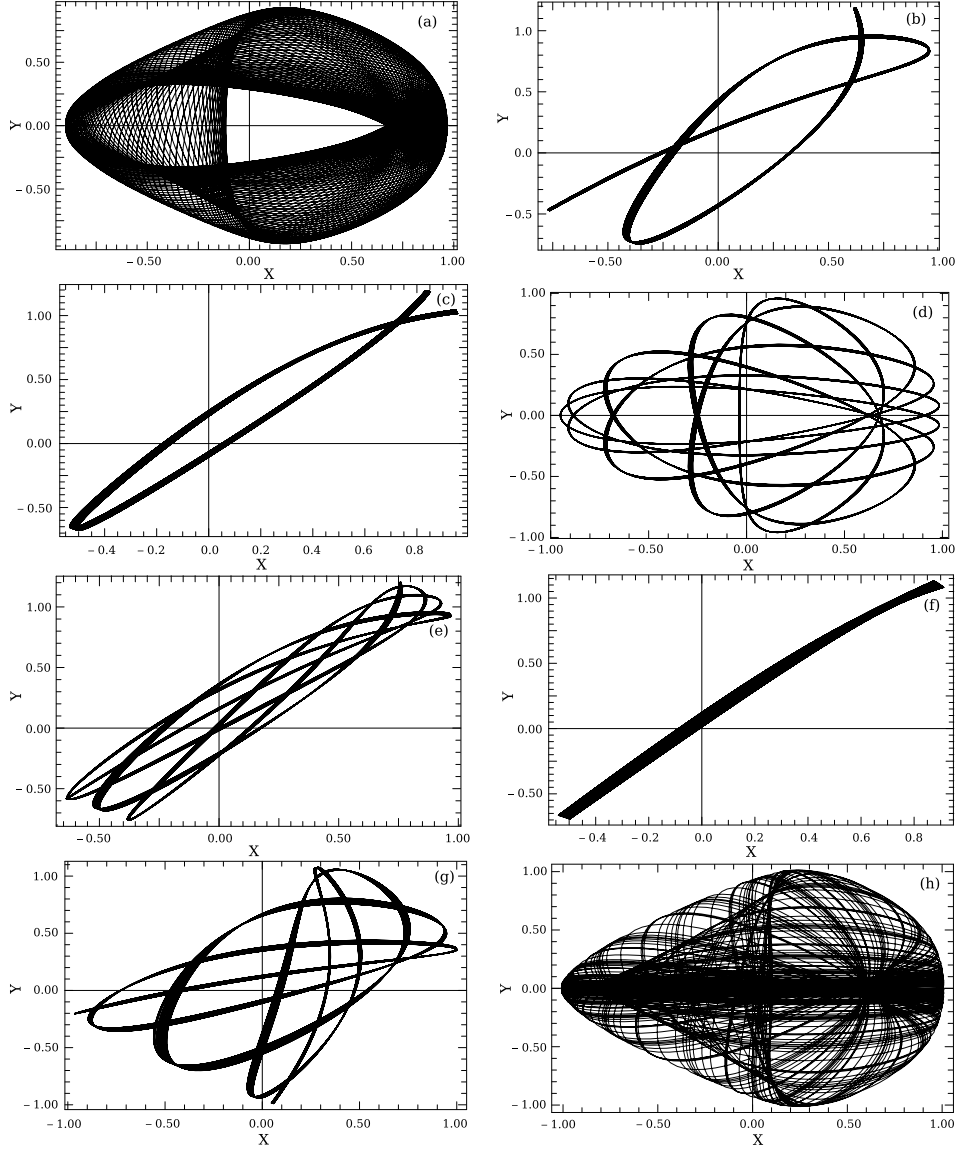


Fig. 2. Orbits in the 2D potential. The initial conditions in panel (a): $x_0 = -0.90$, $p_{x0} = 0$, panel (b): $x_0 = 0.32$, $p_{x0} = 5.2$, panel (c): $x_0 = 0.05$, $p_{x0} = 6.2$, panel (d): $x_0 = -0.952$, $p_{x0} = 0$, panel (e): $x_0 = -0.01$, $p_{x0} = 4.7$, panel (f): $x_0 = -0.01$, $p_{x0} = 6$, panel (g): $x_0 = 0.327$, $p_{x0} = 1.16$, panel (h): $x_0 = 0.09$, $p_{x0} = 0$. In panels (a–e) $M_d = 100$, $E_2 = 20$, in panels (f–h) $M_d = 200$, $E_2 = -10$.

any, is negligible.

Figures 2 (a–h) show several representative orbits in the 2D system. In all orbits $y_0 = 0$, while the value of p_{y0} is always found from the energy integral. The values of initial conditions and parameters are given in the caption. All orbits are

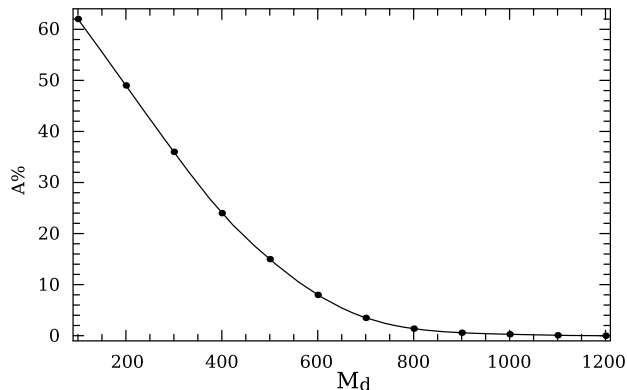


Fig. 3. A plot of the chaotic percentage $A\%$ vs. M_d .

regular except of the orbit given in Figure 2h, which is chaotic. The integration time for all 2D orbits shown in Figures 2 (a–h), is 100 time units.

Thus we conclude, that in elliptical galaxies with massive disks in the central regions a decrease of chaos is expected, while the percentage of chaotic orbits is larger, when a small disk is present. But the most important conclusion drawn from the above numerical study, is that disks in the centers of elliptical galaxies can act as chaos controllers. Figure 3 shows the percentage $A\%$ of the surface of section occupied by chaotic orbits vs. M_d . We see that $A\%$ tends asymptotically to zero, when the mass of the disk increases.

Now let us study the evolution of the sticky orbits of the 2D system. We shall follow in detail the evolution of a sticky orbit with the initial conditions: $x_0 = -0.962$, $p_{x0} = 0$, the values of all other parameters are as in Figure 1a. The results are given in Figure 4 (a–d). Figure 4a shows the sticky region formed in the $x - p_x$ phase plane for a time period of about 1200 time units. After that the test particle leaves the above sticky region, entering to a larger sticky region shown in Figure 4b. There it stays to about 75 000 time units and then it moves to the third sticky region shown in Figure 4c, where it stays until 3×10^5 time units. After reaching this stage, our numerical calculations were not continued. Our feeling is that the evolution of the sticky orbit was completed here. Actually we observe a hierarchy regarding the sticky regions. We believe that in Figure 4c we see a chaotic component of the 2D system, not a sticky region. Figure 4d shows a plot of the LCE of the sticky orbit for a time period of 3×10^5 time units.

A better view of the sticky orbit evolution can be seen using the $S(c)$ spectrum. Figure 5a shows the $S(c)$ spectrum for an orbit producing a set of eight small islands, shown in Figure 1a. The initial conditions are: $x_0 = -0.952$, $y_0 = p_{x0} = 0$, and the values for all other parameters are as in Figure 1a. As expected, we observe eight well defined U -type spectra. The motion is regular. Figure 5b shows the $S(c)$ spectrum for the sticky orbit. Here, we can see again eight spectra, each corresponding to an island. The basic difference between Figures 5a and 5b is that in Figure 5b we observe a large number of asymmetric peaks. Those additional peaks indicate the sticky motion. It is well known, that in the dynamical systems of two degrees of freedom, sticky orbits are the orbits which stay for long time

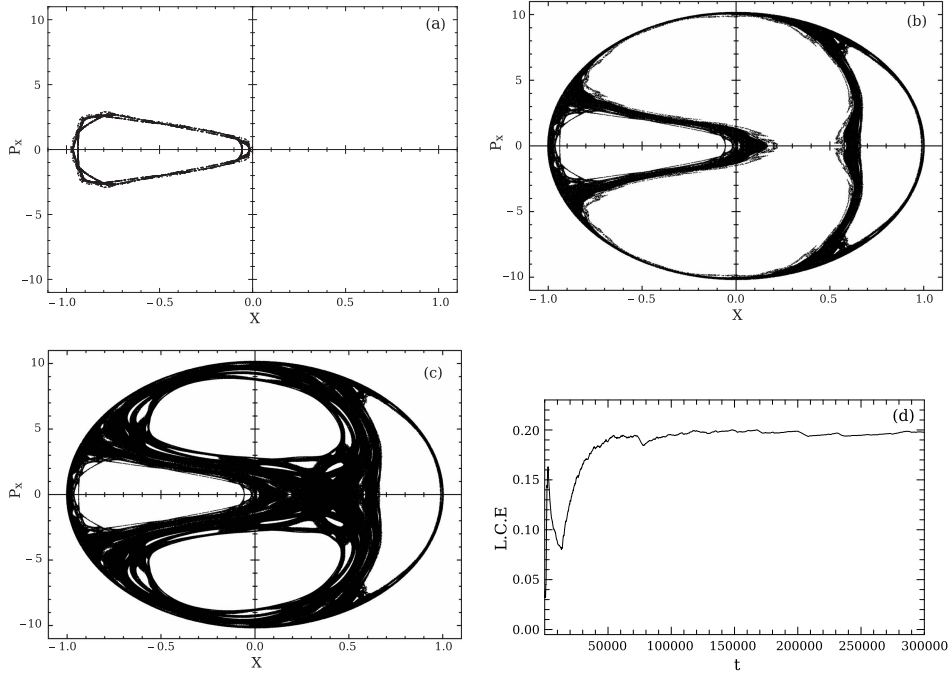


Fig. 4. Panels (a–c): evolution of a sticky orbit; panel (d): LCE vs. time for the sticky orbit.

periods near the last Kolmogorov-Arnold-Moser (hereafter KAM) torus, before they escape to the surrounding chaotic sea (see Karanis & Caranicolas 2002).

According to the Kolmogorov-Arnold-Moser theorem, most orbits lie on tori in the phase space. However, near all unstable periodic points, there is some degree of stochasticity. This is best seen on the surface of section, on which the successive intersections of orbits passing close to the unstable periodic points, do not lie, in general, on closed invariant curves, but fill stochastically a certain defined area. These orbits are called stochastic, or chaotic, or semiergodic. The phenomenon of the onset of large scale chaoticity, has been studied in more detail in recent years. It was found, that the invariant curves that separate chaotic regions in the neighborhood of two unstable periodic orbits are destroyed as the energy goes beyond a critical value. Thus, we have communication between the two chaotic regions. The critical value of the energy occurs when the last KAM curve (or the last KAM torus in the phase plane) separating the two resonant regions is destroyed.

Now let us go to the evolution of the sticky orbit, using the $S(c)$ spectrum. During the first sticky period, which is about 1100 time units, in Figure 5b one observes eight separate complicated spectra. In Figure 5c the time is 1500 time units, and the eight spectra are very similar to those seen in Figure 5b. Note that here the eight spectra are connected. This indicates that the test particle has left the first sticky region in order to continue its wandering in a larger sticky region. Figure 5d, shows the $S(c)$ spectrum for 70 000 time units. We see that the spectrum tends to take characteristics of a chaotic spectrum. Note that the time

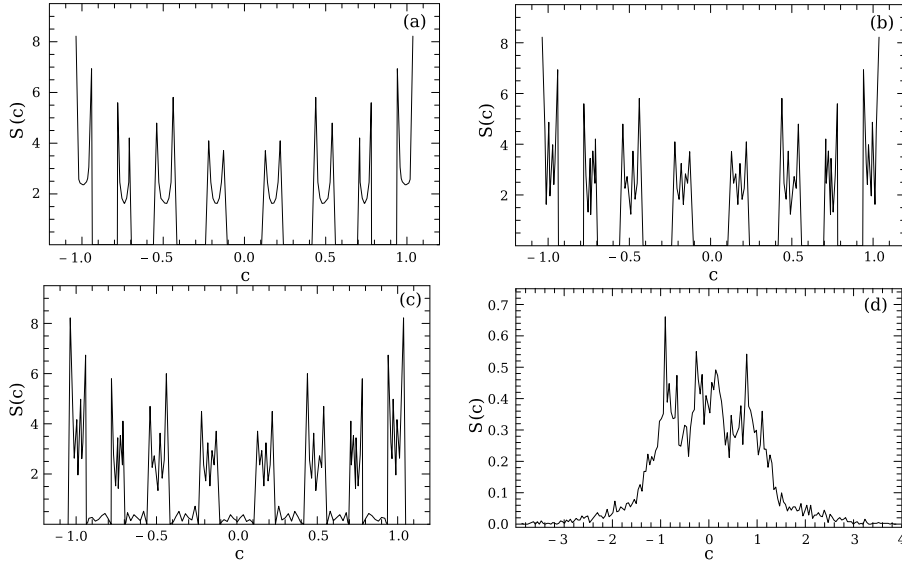


Fig. 5. Panel (a): the $S(c)$ spectrum for an orbit producing the set of eight small islands, shown in Fig. 1a; panels (b-d): evolution of the $S(c)$ spectrum of a sticky orbit. Details are given in the text.

intervals of the sticky periods, obtained by the evolution of the $S(c)$ spectrum, are very close to those obtained by the formation of the $x - p_x$ phase planes, shown in Figures 4 (a-d).

The next step is to investigate different chaotic components of the 2D system. The corresponding results are shown in Figures 6 (a-d). Figure 6a shows the chaotic region formed by an orbit with the initial conditions: $x_0 = 0.0$, $p_{x0} = 4.6$ over a time period of 3×10^5 time units. This is the second chaotic component of the 2D system. Figure 6b shows the third chaotic component which is formed by an orbit with the initial conditions: $x_0 = -0.51$, $p_{x0} = 6.0$. The time period is 3×10^5 time units. Figure 6c shows all the chaotic components together. The LCEs of the above three chaotic components are shown in Figure 6d. The numbers 1, 2 and 3 correspond to the first, second and third chaotic component, respectively. As we see, each chaotic component has a different value of LCE (see Saito & Ichimura 1979). Here we must note that a hierarchical structure in the 2D model is displayed not only by the stickiness but also by chaos.

3. ORDER AND CHAOS IN THE 3D SYSTEM

Now let us switch to study the behavior of the 3D system. We take the initial conditions (x_0, p_{x0}, z_0) , $y_0 = p_{z0} = 0$, where (x_0, p_{x0}) is a point on the phase planes of the 2D system. Obviously this point lies inside the limiting curve

$$\frac{1}{2}p_x^2 + V(x) = E_2 \quad , \quad (5)$$

which is the curve containing all the invariant curves of the 2D system. We take $E = E_2$, and the value of p_{y0} for all orbits is obtained from the energy integral

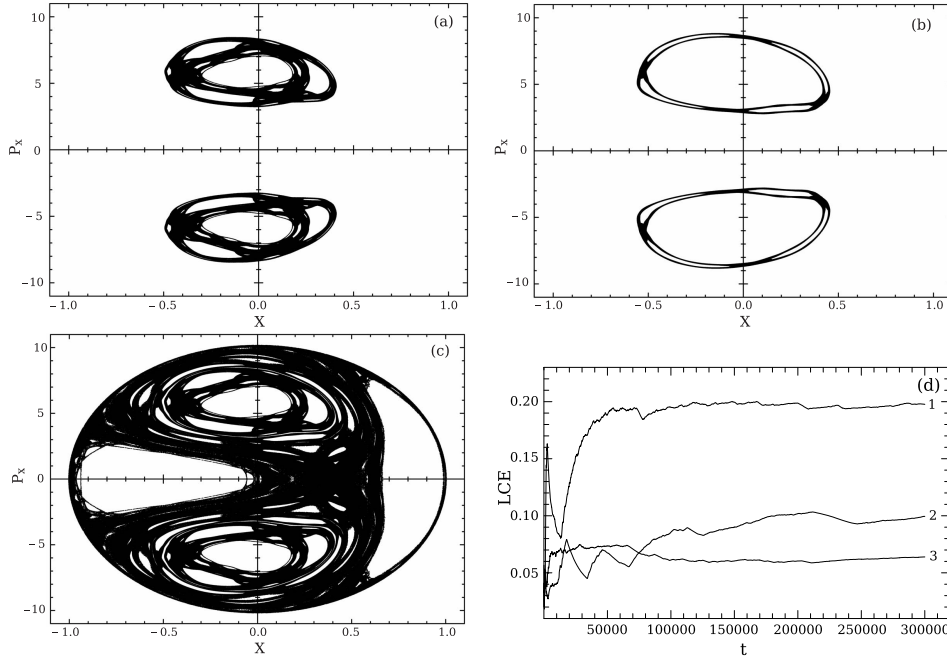


Fig. 6. Panel (a): chaotic component 2; panel (b): chaotic component 3; panel (c): all the chaotic components together; panel (d): the LCEs for the three chaotic components of the 2D system.

(3). Our numerical calculations in the 3D system show, that the orbits with the initial conditions (x_0, p_{x0}, z_0) , $y_0 = p_{z0} = 0$, where (x_0, p_{x0}) is a point in the chaotic regions of Figures 1 (a–d), for all permissible values of z_0 give chaotic orbits. On the other hand, it would be interesting to know what happens with different chaotic components observed in the 2D system, shown in Figures 6 (a–d). The question is, do they merge to form a unified chaotic region in the 3D space, or they continue to exist as three separate chaotic components in the 3D system? In order to give an answer, we computed the LCEs for three orbits, each starting in one of the three different chaotic components, for a time period of 10^6 time units. The results are shown in Figure 7. The numbers 1, 2 and 3 indicate the three chaotic components which have different LCEs values. This result seems to be consistent with the outcomes obtained by Cincotta et al. (2006), where in a 3D system with divided phase space, separate chaotic components actually exist.

One may ask an interesting question: what is the nature of orbits which have initial conditions (x_0, p_{x0}, z_0) , $y_0 = p_{z0} = 0$, where (x_0, p_{x0}) is a point in each regular region of Figures 1 (a–d)? In order to give an answer, we will introduce and use a new type of dynamical indicator, the $S(w)$ spectrum. The parameter w_i is defined as

$$w_i = \frac{(x_i - p_{xi}) - (z_i - p_{zi})}{p_{yi}}, \quad (6)$$

where $(x_i, z_i, p_{xi}, p_{yi}, p_{zi})$ are the successive values of (x, z, p_x, p_y, p_z) of the 3D

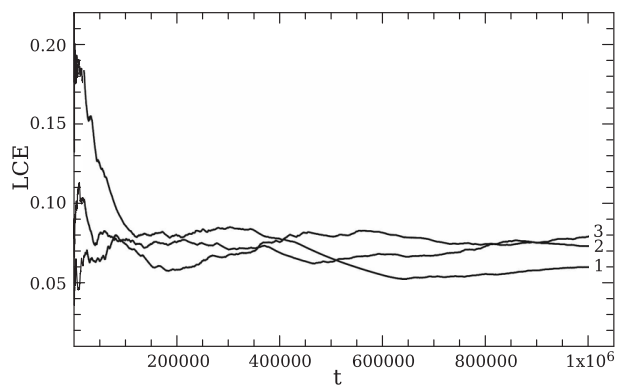


Fig. 7. The LCEs for the three chaotic components of the 3D model.

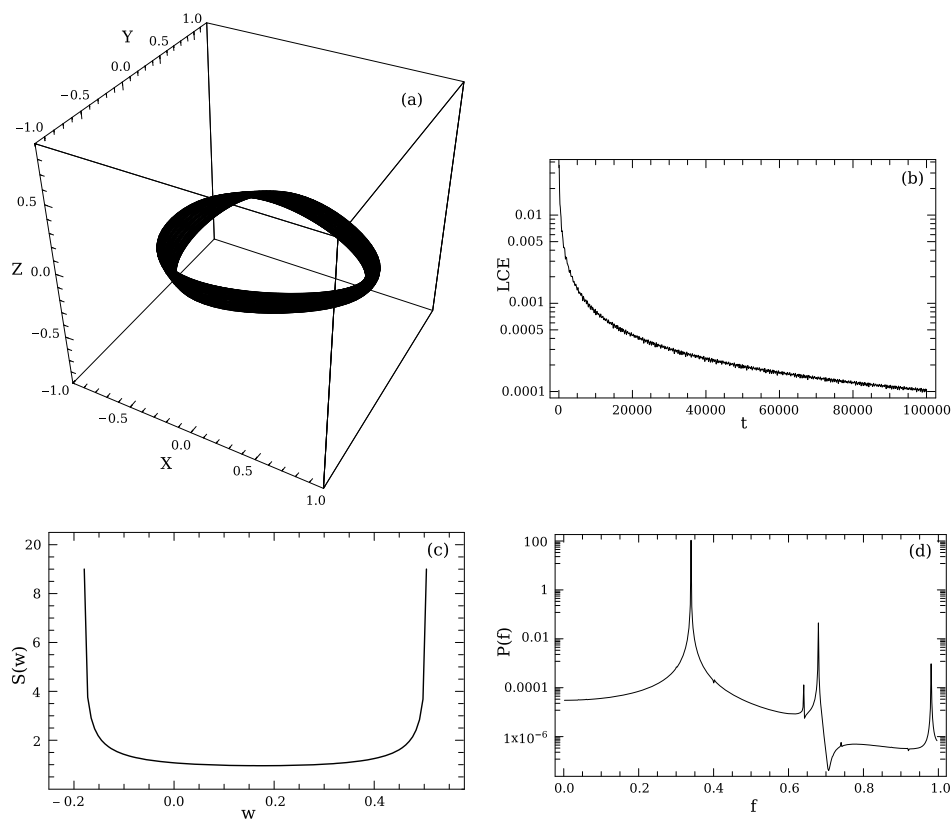


Fig. 8. Panel (a): a 3D regular orbit; panel (b): a plot of the LCE vs. time for the orbit shown in (a); panel (c): the $S(w)$ spectrum of the orbit shown in (a); panel (d): the $P(f)$ indicator for the orbit shown in (a). See the text for details.

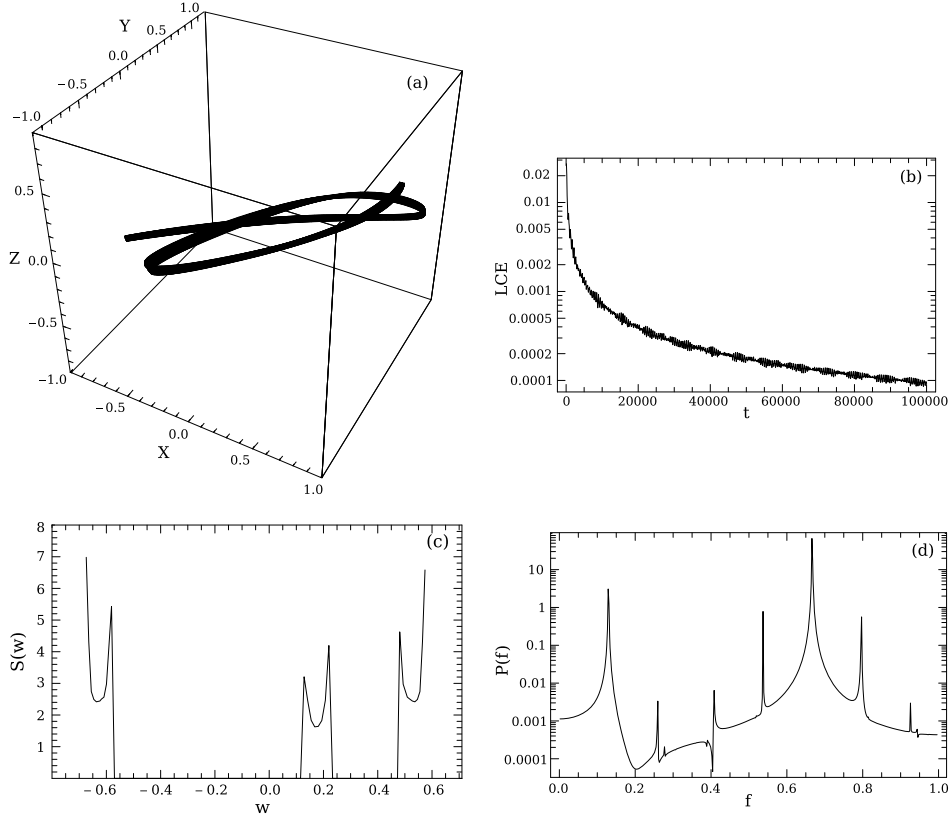


Fig. 9. The same as in Figures 8 (a–d) but for a resonant 3D orbit. See the text for details.

orbit. The dynamical spectrum of the parameter w is its distribution function

$$S(w) = \frac{\Delta N(w)}{N \Delta w} \quad , \quad (7)$$

where $\Delta N(w)$ is the number of the parameters w in the interval $w, w + \Delta w$ after N iterations. In order to study the character of a 3D orbit, the $S(c)$ spectrum can be also used. Note that the coupling of the third component, z , carrying all the information about the 3D motion, is hidden in the definition of the $S(c)$ spectrum, but in any case it affects the values of x, p_x and p_y . Using the definition of the $S(w)$ spectrum, we overtake this minor drawback and create a new dynamical spectrum, suitable especially for 3D orbits.

Figures 8 (a–d) show the results for a 3D regular orbit. The orbit which is shown in Figure 8a has the initial conditions: $x_0 = 0.82, y_0 = p_{x0} = p_{z0} = 0, z_0 = 0.01$, while for all 3D orbits the value of p_{y0} is always found from the energy integral (3). The corresponding values of all other parameters are as in Figure 1a. The LCE of the orbit, shown in Figure 8b, vanishes indicating the regular motion. Figure 8c shows the $S(w)$ spectrum of the orbit. This is a well defined U-type spectrum characteristic for the regular motion. In Figure 8d, we see the $P(f)$ indicator which also indicates the regular motion. Figures 9 (a–d) are similar to

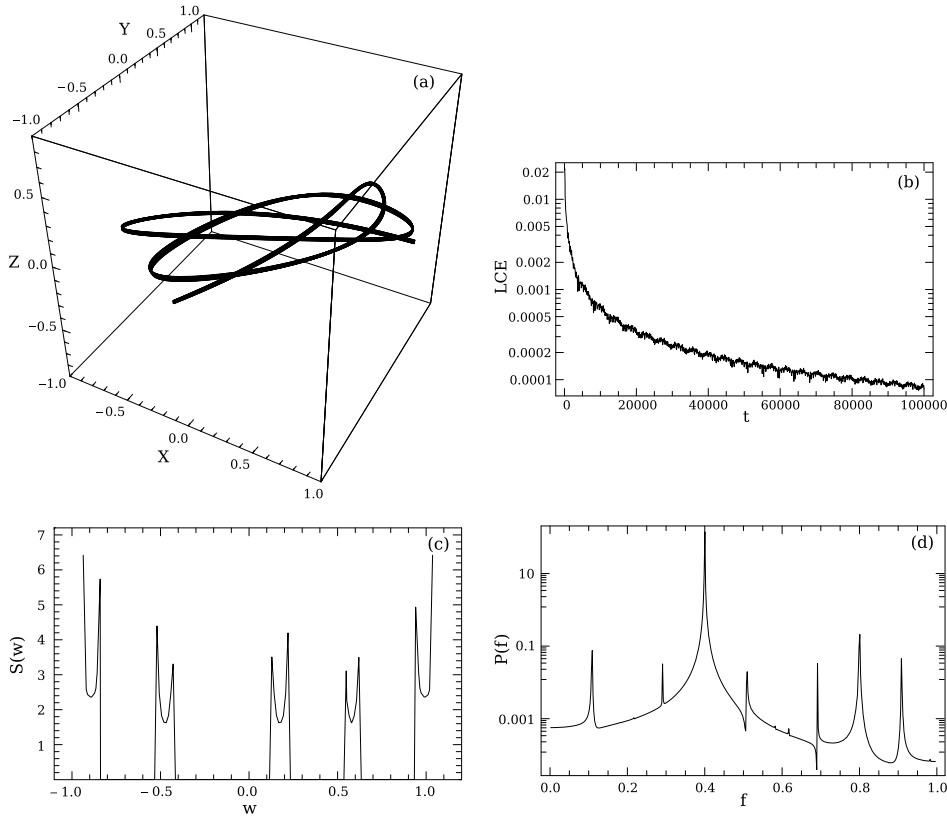


Fig. 10. The same as in Figures 9 (a–d) but for a resonant 3D orbit with different initial conditions. See the text for details.

Figures 8 (a–d) but correspond to a 3D resonant orbit with the initial conditions: $x_0 = 0.27$, $y_0 = p_{z0} = 0$, $p_{x0} = 5.3$, $z_0 = 0.01$, producing three U -type spectra. The values of all other parameters are as in Figure 1b.

Figures 10 (a–d) are similar to Figures 9 (a–d) but for a 3D resonant orbit with the initial conditions: $x_0 = 0.47$, $y_0 = p_{z0} = 0$, $p_{x0} = 4.9$, $z_0 = 0.01$, producing five U -type spectra. The values of all other parameters are as in Figure 1b. Finally, in Figure 11 (a–d), we present the results for a 3D chaotic orbit. The initial conditions are: $x_0 = 0.09$, $y_0 = p_{x0} = p_{z0} = 0$, $z_0 = 0.1$. The values of all other parameters are as in Figure 1a. Once more, we observe that the results from all dynamical indicators, regarding the character of motion, coincide. The integration time for all 3D orbits is 100 time units, for the $S(w)$ spectrum it is 2×10^4 time units and for the $P(f)$ indicator it is 4×10^3 time units.

Using the above method, we have computed a large number of orbits (about 1000) in the 3D dynamical system. Numerical outcomes suggest that for all (x_0, p_{x0}) in the regular regions of Figures 1 (a–d) and for small values of z_0 ($z_0 \lesssim 0.12$) the motion is regular, while for all larger permissible values of z_0 the motion becomes chaotic.

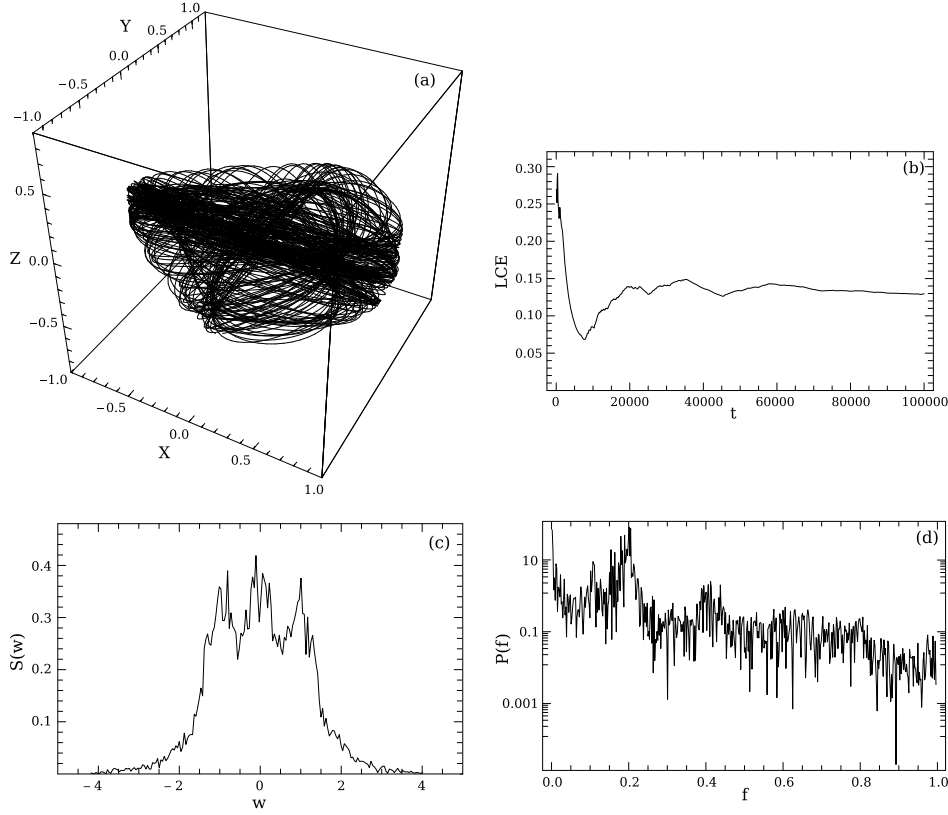


Fig. 11. The same as in Figures 8 (a–d) but for a chaotic 3D orbit. See the text for details.

4. DISCUSSION AND CONCLUSIONS

In this article we have studied the properties of motion in a 3D Hamiltonian system, describing the motion in the inner parts of a deformed galactic model. We started our investigation from the 2D system, because orbits confined in the galactic plane ($z = 0$) display some very interesting features, such as sticky regions, chaotic components and islandic motion produced by a large number of secondary resonances.

Results from the study of the phase planes indicate, that there is an hierarchy in sticky regions. A test particle can stay in sticky regions for a time period of about 75 000 time units, before leaving to the corresponding chaotic region. Several chaotic components are also observed in the 2D system, each one having a different value of LCE. Thus we conclude, that both the stickiness and chaos display a hierarchical structure in the 2D model. An interesting result of this investigation is that the percentage $A\%$ of the surface of the section occupied by chaotic orbits decreases, tending asymptotically to zero, when the mass of the disk increases. This suggests that disks in elliptical galaxies can act as the chaos controllers.

Our numerical calculations in the 3D system show, that orbits with the initial

conditions (x_0, p_{x0}, z_0) , $y_0 = p_{z0} = 0$, where (x_0, p_{x0}) is a point in the chaotic regions of Figure 1 (a–d), for all permissible values of z_0 give chaotic orbits. Using the new $S(w)$ spectrum we find that orbits with the initial conditions (x_0, p_{x0}, z_0) , $y_0 = p_{z0} = 0$, where (x_0, p_{x0}) is a point in the regular regions of Figure 1 (a–d), for small values of z_0 are regular, while for larger values of z_0 they become chaotic. It is also of particular interest that the 3D system displays three different chaotic components, not a unified chaotic region.

A very effective and reliable tool to distinguish between the regular and chaotic motion in the 3D dynamical systems is the new $S(w)$ spectrum. This spectrum, which is an advanced form of the $S(c)$ spectrum, allows us to detect islandic 3D motion of the resonant orbits, since it produces as much spectra as the total number of islands in the $x - p_x, y = 0, p_y > 0$ surface of section (see Figures 9a and 10a). Moreover, the comparison with other dynamical parameters, such as the LCE and the $P(f)$ indicator, shows that the results obtained by the $S(w)$ spectrum are reliable.

ACKNOWLEDGMENTS. The author would like to thank Prof. N. D. Caranicolas for his fruitful discussions during this research. I also would like to thank Peeter Tenjes for careful reading of the manuscript and useful comments which allowed us to improve the quality of the paper.

REFERENCES

- Barazza F. D., Binggeli B., Jerjen H. 2002, *A&A*, 391, 823
 Binggeli B., Tamman G. A., Sandage A. 1987, *AJ*, 94, 251
 Caranicolas N. D., Papadopoulos N. 2007, *AN*, 328, 556, 259
 Caranicolas N. D., Zotos E. E. 2010, *New Astronomy*, 15, 427
 Cincotta P. M., Giordano C. M., Perez M. J. 2006, *A&A*, 455, 499
 Conselice C. J., Gallagher J. S. III, Wyse R. F. G. 2001, *ApJ*, 559, 791
 Contopoulos G., Polymilis C. 1993, *Phys. Rev. E*, 46(3), 1546
 Contopoulos G., Varvoglis H., Barbanis B. 1987, *A&A*, 172, 55
 De Rijcke S., Dejonghe H., Zeilinger W. W., Hau G. K. T. 2001, *ApJ*, 559, 21
 Feruson H. C., Sandage A. 1989, *ApJ*, 346, 53
 Jerjen H., Kalnajs A., Binggeli B. 2000, *A&A*, 358, 845
 Karanis G. I., Caranicolas N. D. 2002, *AN*, 323, 3
 Karanis G. I., Vozikis Ch. L. 2008, *AN*, 329, 403
 Khochfar S., Burkert A. 2005, *MNRAS*, 359, 1379
 Lichtenberg A. J., Leiberman M. A. 1992, *Regular and Chaotic Dynamics*, 2nd Edition, Springer
 Mayer L., Governato F., Colpi M. et al. 2001, *ApJ*, 547, 123
 Merrifield M. R., Kuijken K. 1999, *A&A*, 345, L47
 Miyamoto W., Nagai R. 1975, *PASJ*, 27, 533
 Moore B., Lake G., Katz N. 1998, *ApJ*, 495, 139
 Ryden B. S., Terndrup D. M., Pogge R. W. 1999, *ApJ*, 517, 650
 Saito N., Ichimura A. 1979, in *Stochastic Behaviour in Classical and Quantum Hamiltonian Systems*, eds. G. Casati & L. Ford, Springer, p. 137
 Simien F., Prugniel Ph. 2002, *A&A*, 384, 371
 Siopis C., Contopoulos G., Kandrup H. E. 1995, *NYASA*, 751, 205
 Young L. M. 2002, *AJ*, 124, 788
 Young L. M. 2005, *ApJ*, 634, 258